HEAT TRANSFER APPRAISING AND SECOND LAW ANALYSIS OF CuWATER NANOLIQUID FILLED MICROCHANNEL: SLIP FLOW REGIME

MOKHTAR FERHI[1] and RIDHA DJEBALI[2]

[1] University of Tunis, Higher National Engineering School of Tunis, Department of Industrial Engineering and Applied Physics, 1008 Tunis, Tunisia
E-mail: moktar.ferhi@gmail.com or moktar.ferhi@ensit.rnu.tn
[2] University of Jendouba, ISLAI Béja, Department of Computer Sciences, 9000 Béja, Tunisia
E-mail: jbelii_r@hotmail.fr or ridha.djebali@islaib.u-jendouba.tn

Received September 26, 2021

Abstract. The purpose of this article is twofold. Firstly, the objective is to evaluate the ability of the *Lattice Boltzmann method* (LBM) to manipulate flows and heat transfers in micro geometries, namely micro flows. Secondly, the study aims to perform a second law analysis for the case of partially heated horizontal microchannel filled with Cu – water in the slip flow regime by means of the LBM method. The slip velocity and the temperature jump conditions are applied to lower and upper walls. The problem parameters effects in the margins: nanoparticles volume fraction (ϕ = 0–4%), Reynolds number (Re = 10–100) and Knudsen number (Kn = 0–0.1) on flow structure, heat transfer rate, slip velocity, temperature jump and entropy generation were reported. The obtained results show that the increase of ϕ, Re and Kn improves the heat transfer rate, except for high Re values. The average Nusselt number (Nu) decreases beyond Kn = 0.8. The heat transfer rate inside the microchannel depends greatly on the nanoparticles size. The total entropy generation decreases as ϕ and Kn increase. In contrast, the slip velocity and the temperature jump increase with Kn.

Key words: Microchannel, nanofluid, entropy generation, slip velocity, temperature jump.

1. INTRODUCTION

Micro-device technology has become an interesting and a motivating research field in the last few decades, due to the great development in *micro/nano-electro-mechanical systems* (MEMS/NEMS) and its extensive applications in different fields. The transport phenomena and convective heat transfer in micro flow are found in a vast variety of emerging biomedical diagnosis, cooling of electronic devices, biochemical engineering.

The Knudsen number Kn is a key parameter that characterizes flows on microscopic scale. The number Kn is defined as the ratio of the mean free path and the length of the studied micro geometry. The flows regimes are classified into four

types [1–4]: The continuum regime ($Kn < 10^{-3}$), the slip regime ($10^{-3} < Kn < 10^{-1}$), the transitional regime ($10^{-1} < Kn < 10$) and the molecular regime ($Kn > 10$).

Tackling the investigation of the thermofluidic characteristics of microflow has been the subject of many research efforts. Elgannouni *et al.* [5] used the *Thermal Lattice Boltzmann Method* (TLBM) to analyze the hydrodynamic and thermal characteristics of two cases of micro-Poiseuille flow driven by a constant inlet velocity. The first case consisted of a micro flow with uniform temperature at the walls (equal to zero) and a hot temperature at the inlet. However, in the second case, the gas flow is generated by the decrease effect of temperature at the walls. In both cases slip velocity and temperature jump conditions are used. It has been proven that the key parameter used for simulating gas microflow; which is the Knudsen number; has a great influence on the isotherms, velocity and temperature profiles, and Nusselt number.

Afrouzi *et al.* [6] performed a numerical investigation on the effect of viscous dissipation of forced convection in a microchannel filled with Al_2O_3/water nanofluid and subjected to an ascending non-uniform magnetic field using the *Lattice Boltzmann Method* (LBM). Both slip velocity and temperature jump are used again. Authors have asserted that the volume fraction and Hartmann number tend to increase the friction coefficient and the Nusselt number. In addition, the rise in dimensionless slip coefficient B reduces the friction coefficient and the centerline velocity. On the other hand, the increase in the Hartmann number tends to diminish the centerline velocity and improve the friction coefficient.

Kalteh and Abedinzadeh [7] investigated numerically by means of LBM *Magnetohydrodynamic* (MHD) forced convection in a two-dimensional microchannel filled with Al_2O_3–water nanofluid. The temperature of microchannel lower wall is kept constant, while the upper wall is insulated. It was found that the increase of nanoparticles volume fraction enhances the heat transfer rate with 17%. The heat transfer coefficient is improved by the augmentation of the convective effects. They have noticed that the magnetic field has a great influence on the friction factor but does not significantly affect the heat transfer rate.

Afrand *et al.* [8] examined the effects of slip velocity and uniform vertical magnetic field in a parallel plate microchannel filled with FMWCNT–water nanofluid using the *finite volume method* (FVM). The nanoliquid is driven by a constant velocity and hot temperature at the inlet. The temperature of the microchannel entrance wall is insulated but the rest of the length is kept constant. It was once again proved that the slip velocity grows and the centerline velocity undergoes a reduction with increasing the slip coefficient and the Hartmann number. The effect of slip coefficient is remarkable with change of Hartmann (Ha) numbers. The convective effects and the magnetic field improve the heat transfer rate. Karimipour *et al.* [9] studied the effect of MHD and slip velocity on forced convection nanofluids in a microchannel with constant heat flux at a part of the upper wall. The insulated condition is applied at all other microchannel flow.

Authors have concluded that the rise in the slip coefficient increases both the slip velocity and the heat transfer rate while it decreases the centerline velocity. The increase in the magnetic field strength leads to the slip velocity development. The imposed transverse magnetic field has thus a significant effect on the heat transfer efficiency in the thermally developing region.

Karimipour and Afrand [10] used the FVM to perform the MHD forced convection nanofluids on the slip velocity and temperature jump in a two-dimensional microchannel. Authors have concluded that the Hartmann number has a great influence on the slip velocity and a negligible effect on the temperature jump. The augmentation in slip coefficient increases the slip velocity and temperature jump. The heat transfer rate depends strongly on Re, Ha and u. Besides, the effects of Ha and u are pronounced for higher convective force.

Karimipour *et al.* [11] investigated numerically the fluid flow and heat transfer in a long microchannel under the effect of vertical magnetic field using the finite volume approach. Both slip velocity and temperature jump conditions are applied near the horizontal walls. The effects of ceramic (Al_2O_3) and metallic (Ag) nanoparticles were investigated. Researchers have proved that the increase in slip coefficient reduces Nusselt number and increases the slip velocity especially at higher Hartmann numbers. Therefore, it has been recommended using ceramic nanofluid in order to enhance the heat transfer rate from the microchannel.

Karimipour [12] performed a numerical study in a microchannel filled with Ag, Al_2O_3, and Cu/water nanofluids using LBM. The specular reflective bounce back model [13] and diffusive scattering boundary condition [14] are applied for the slip velocity and temperature jump conditions, respectively. Researchers recommended applying nanofluid with a lower value of slip coefficient and higher value for the nanoparticles volume fraction and Prandtl number (Pr) to enhance the heat transfer rate.

Zhang *et al*. [15] explored numerically the effects of buoyancy force and thermal boundary condition on mixed convection in different models of microchannel using the LBM. The specular reflective bounce back model [13] is applied for the slip velocity and *general purpose thermal boundary condition* (GPTBC) [16] is used to simulate temperature jump condition. Researchers have argued that the buoyancy force affects the velocity distribution at the inlet region. At higher Grashof number (Gr), a negative velocity is generated by the formation of the backflow. This feature facilitates the heat transfer near the top wall for all studied models. The thermal performance is most positive for the case when the top wall is heated.

Mozaffari *et al.* [17] studied the nanofluid mixed convection in a microchannel using LBM. The flow is induced by a constant temperature at the walls, equal to 1, uniform velocity and cold condition for temperature at the inlet. The micro aspect is highlighted based on the slip velocity and temperature jump conditions applied to the horizontal microchannel walls. It has been deduced that the growth in the slip coefficient leads to an increase in the slip velocity and

temperature jump, which reach their maximum in the input region. It has also been noticed that the introduction of the gravity term in the Boltzmann equation creates powerful buoyancy motions at the input area. This feature changes the slip velocity and friction coefficient of the microflow. Mozaffari *et al.* [18] used the LBM to perform a relatively similar study to Mozaffari *et al.* [17], but with constant heat flux at the wall boundaries. The addition of the term of gravity in the Boltzmann equation as an external force has shown the latter's effect on different inclination angles of the microchannel. The gravity affects the hydrodynamic and thermal proprieties of the flow. Besides, the velocity and temperature goes up with respect to inclination angle and Kn. The heat transfer rate depends strongly on the augmentation of Gr numbers.

Zarita and Hachemi [19] used the LBM to analyze the heat transfer enhancement in a microchannel filled with Ag-water nanofluid. The results have shown that increasing Kn number leads to an increase of the slip velocity and reduction of the local heat transfer which consequently reduces the friction coefficient C_f Re. It has been also found that the increase in Kn number reduces the heat transfer rate.

Raisi *et al.* [20] used the FVM to investigate the forced convection in a microchannel crossed Cu-water nanofluid. The middle section walls are heated with a constant temperature, while the rest of the walls are insulated. The microflow is generated by a constant velocity and cold temperature at the inlet. Remarkably, the slip coefficient reveals no considerable effect on the heat transfer at low Re numbers, whereas at high Re numbers the increase in the slip coefficient increases the heat transfer rate.

Arabpour *et al.* [21] use the FVM to study the effect of slip velocity on the fluid flow and heat transfer of MWCNT-kerosene nanofluid in a double layer microchannel. They found that by raising the Re, the nanoparticles volume fraction and the slip coefficient, the wall thickness decreases and the Nusselt number multiplies.

Monaledi and Makinde [22] appraise the effect of nanoparticle injection and distribution on entropy generation of a microchannel crossed with Cu-water nanofluid using the modified Buongiorno's nanofluid model. The obtained results show that the nanofluid generates more entropy as compared to the base fluid, while the Bejan number is more important for the base fluid. Entropy production is more visible at the walls and less along the microchannel core region. As γ, Le, N_b and Ec grow, entropy generation rate raises, while an increase in N_t reduces the entropy production. Bejan number undergoes a reduction with γ and N_b but multiply with N_t.

Sindhu *et al*. [23] used the Runge–Kutta–Fehlberg integration scheme to examine the influence of radiation on nanoliquid flow through a vertical microchannel in the presence of heat source. The obtained results show that the entropy generation rate decline with the slip parameter A. The increase of Bi

results to higher entropy of the nanoliquid. Similarly the increase of Br enhances the total entropy inside the microchannel. The significant improvement in entropy generation occurs when greater values of H. Bejan number grow across the microchannel with greater values of Bi. Finally, Lamina-shaped MWCNT has higher Bejan number.

Al-Rashed *et al.* [24] investigated numerically the entropy generation of a non-Newtonian nanofluid containing CuO nanoparticles in an offset strip-fin *microchannel heat sink* (MCHS). Results have revealed that the increase of the Re from100 to 300, and the significant decline of the total entropy generation rate. However, augmenting Re (Re > 300) leads to a rise of the total entropy generation rate.

For motivating researchers in the domain of micro-thermal systems, Huminic and Huminic [25] performed a comprehensive review on the entropy generation in different configurations (microchannels, minichannels, and cavities) using nanofluids/hybrid nanofluids. Awad [26] reported a review on the entropy generation on microchannels and includes recommendations for future studies in this field.

The contemporary study aims to numerically examine the flow, convective heat transfer and S_{gen} analysis in the case of a uniquely heated microchannel crossed with Cu/water in the slip flow regime. The slip velocity and the temperature jump conditions are used to incorporate the micro aspect. The Brownian motion is considered in the nanofluid thermal conductivity model. The flow and heat transfer characteristics, and the irreversibility are thoroughly investigated in terms of various dimensionless independent variables such as: nanoparticles volume fraction, diameter size, Re and Kn numbers.

2. PROBLEM STATEMENT

The physical problem of the current study consists of a two-dimensional microchannel of width L and height H (L/H = 4) (Figure 1). The nanofluid flow is driven along the microchannel by a constant velocity and a cold temperature at the inlet (U_{in} and T_{in}; respectively). Parts of the microchannel walls, located near the entrance, the middle, and at the outlet of the microchannel, are insulated. At the remaining parts, the microflow is induced by the effect of a uniform temperature which is equal to one (T_H).

3. MATHEMATICAL FORMULATION AND BOUNDARY CONDITIONS

The flow and heat transfer in the microchannel crossed with Cu-water nanofluid are governed by the non-dimensional Navier–Stokes coupled with the energy equations [20]:

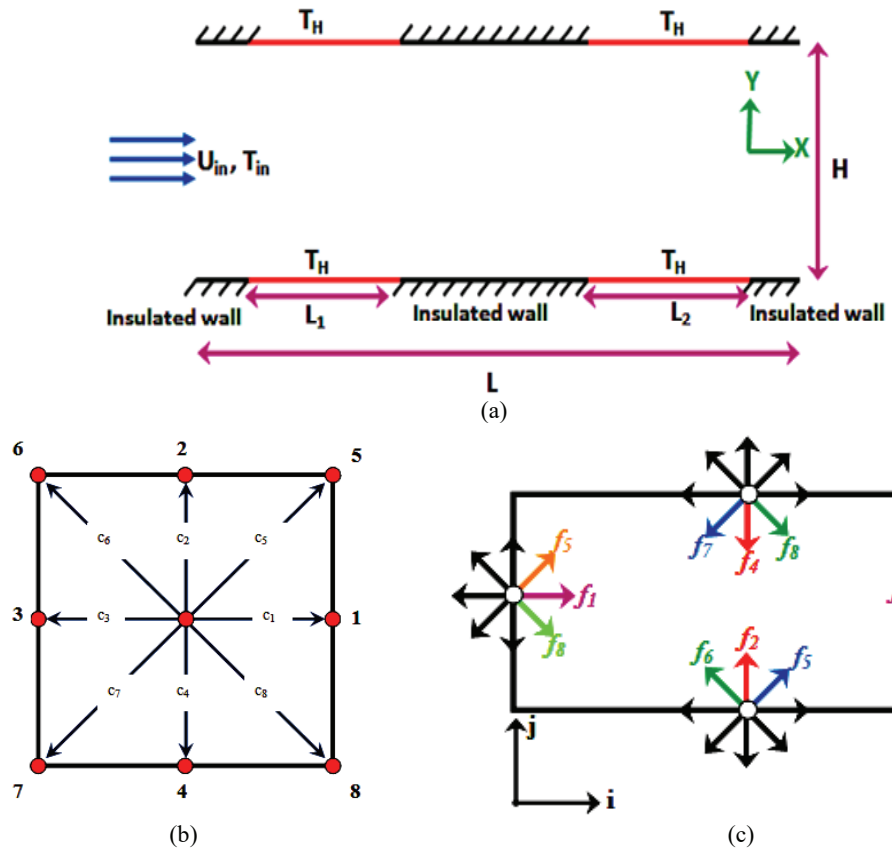

Fig. 1 – Scheme of studied configuration (a), the D_2Q_9 model (b) and the distribution functions (c) in the boundaries of the microchannel.

Continuity equation

$$\frac{\partial U}{\partial X}+\frac{\partial V}{\partial Y}=0 \tag{1}$$

Momentum equation

$$U\frac{\partial U}{\partial X}+V\frac{\partial U}{\partial Y}=-\frac{\partial P}{\partial X}+\frac{\mu_{nf}}{\rho_{nf}\upsilon_f}\frac{1}{\mathrm{Re}}\left(\frac{\partial^2 U}{\partial X^2}+\frac{\partial^2 U}{\partial Y^2}\right) \tag{2}$$

$$U\frac{\partial V}{\partial X}+V\frac{\partial V}{\partial Y}=-\frac{\partial P}{\partial Y}+\frac{\mu_{nf}}{\rho_{nf}\upsilon_f}\frac{1}{\mathrm{Re}}\left(\frac{\partial^2 V}{\partial X^2}+\frac{\partial^2 V}{\partial Y^2}\right) \tag{3}$$

Energy equation

$$U\frac{\partial \theta}{\partial X}+V\frac{\partial \theta}{\partial Y}=\frac{\alpha_{nf}}{\alpha_f}\frac{1}{\mathrm{Re}\,\mathrm{Pr}}\left(\frac{\partial^2\theta}{\partial X^2}+\frac{\partial^2\theta}{\partial Y^2}\right) \tag{4}$$

Near the horizontal walls, the modeling of the flow and heat transfer need to apply the slip velocity and temperature jump conditions in its dimensional forms ([27, 5, 19]):

$$u_{\mathrm{y=0}}^{slip}=u_{x,\mathrm{y=0}}-u_{x,\mathrm{paroi}}=\sigma\mathrm{Kn}\left(\frac{\partial u}{\partial y}\right)_{y=0} \tag{5}$$

$$u_{\mathrm{y=H}}^{slip}=u_{x,\mathrm{paroi}}-u_{x,\mathrm{y=H}}=\sigma\mathrm{Kn}\left(\frac{\partial u}{\partial y}\right)_{y=H} \tag{6}$$

$$T_{\mathrm{x},y=0}^{\mathrm{jump}}=T_{x,\mathrm{y=0}}-T_{x,\,\mathrm{paroi}}=\zeta\mathrm{Kn}\left(\frac{2\gamma}{(\gamma+1)Pr}\right)\left(\frac{\partial T}{\partial y}\right)_{y=0} \tag{7}$$

$$T_{\mathrm{x},y=\mathrm{H}}^{\mathrm{jump}}=T_{x,\,\mathrm{paroi}}-T_{x\,\mathrm{y=H}}=\zeta\mathrm{Kn}\left(\frac{2\gamma}{(\gamma+1)Pr}\right)\left(\frac{\partial T}{\partial y}\right)_{y=\mathrm{H}} \tag{8}$$

σ, ξ , γ, Kn and Pr are respectively, the tangential momentum accommodation coefficient, the thermal accommodation coefficient, the specific heat transfer ratio, Knudsen number and Prandtl number.
At the inlet:

$$\mathrm{U}=\mathrm{U_{in}},\ \mathrm{T}=\mathrm{T_{in}}=0 \tag{9}$$

At the outlet:

$$\frac{\partial \mathrm{U}}{\partial \mathrm{Y}}=\frac{\partial \mathrm{V}}{\partial \mathrm{Y}}=\frac{\partial \mathrm{T}}{\partial \mathrm{Y}}=0 \tag{10}$$

4. NUSSELT NUMBER CALCULATION

Heat transfer characteristic of the microflow can be determined using the Nusselt number. The Nusselt number in its local form along the horizontal bottom wall of the microchannel is calculated as follows:

$$\mathrm{Nu_b}=-\frac{\mathrm{k_{nf}}}{\mathrm{k_f}}\left(\frac{\partial \mathrm{T}}{\partial \mathrm{Y}}\right)_{\mathrm{X=0}} \tag{11}$$

Therefore, the average Nusselt number is calculated as follows:

$$\overline{\mathrm{Nu_b}} = -\frac{1}{\mathrm{L}}\frac{\mathrm{k_{nf}}}{\mathrm{k_f}}\int_0^{\mathrm{L}}\left(\frac{\partial \mathrm{T}}{\partial \mathrm{Y}}\right)_{\mathrm{X=0}} \tag{12}$$

5. ENTROPY GENERATION

The local dimensionless entropy generation is the results of the sum of the *irreversible heat transfer* (HTI) and *fluid friction* (FFI) [28–32].

$$S_{gen\_local} = \mathrm{HTI} + \mathrm{FFI} \tag{13}$$

$$S_{gen\_local} = \left\{\frac{\partial^2\theta}{\partial X^2} + \frac{\partial^2\theta}{\partial Y^2}\right\} + \zeta_1\left\{2\left[\left(\frac{\partial U}{\partial X}\right)^2 + \left(\frac{\partial V}{\partial Y}\right)^2\right] + \left(\frac{\partial U}{\partial Y} + \frac{\partial V}{\partial X}\right)^2\right\} \tag{14}$$

The irreversibility distribution ratio and the local Bejan number are defined as:

$$\zeta_1 = \frac{\mu_{hnf} T_0}{k}\left(\frac{\alpha}{H\Delta T}\right)^2 = 10^{-5} \tag{15}$$

$$\mathrm{Be}_{local} = \frac{\mathrm{HTI}}{S_{gen\_local}} \tag{16}$$

The total entropy generation, S_{gen} and the Bejan number, Be are calculated by the integration over the whole domain Ω as:

$$S_{gen} = \iint_{\Omega} S_{gen\_local}\ \mathrm{d}X\mathrm{d}Y \text{ and } \mathrm{Be} = \iint_{\Omega} \mathrm{Be}_{local}\ \mathrm{d}X\mathrm{d}Y \tag{17}$$

The Bejan number Be is a parameter reflecting the importance of heat transfer irreversibility in the domain. When Be > 0.5, Be < 0.5, HTI and the FFI are the dominant.

6. NUMERICAL METHOD

To simulate flow and heat transfer in a microchannel the *Lattice Boltzmann Method* (LBM) is used with the D_2Q_9 model (Figure 1b) for both dynamic and thermal fields [33–40]. The lattice Boltzmann method has been used successfully in various classic and emerging scientific and engineering fields and has proven a powerfulness to pose an alternative to classical discretization methods [41–45].

6.1. LATTICE BOLTZMANN EQUATION

After introducing the BGK approximation, the LB equation with external term force is solved. Consequently, the distribution function is written as:

$$f_i\left(x+\mathrm{c_i}\Delta t,t+\Delta t\right)=f_i\left(x,t\right)+\frac{\Delta t}{\tau}\left[f_i^{eq}\left(x,t\right)-f_i\left(x,t\right)\right]+\Delta \mathrm{tF_i} \tag{18}$$

where Δt, c_i, F_i and $f_\mathrm{i}^{\mathrm{eq}}$ denotes respectively the lattice time step, the discrete lattice velocity in direction i, the external force in direction of lattice velocity (c_i), the relaxation time and the equilibrium distribution function.

The LBM utilize two distribution functions, f and g in both flow and temperature fields; the equilibrium distribution functions are calculated as follows:

$$f_i^{eq}=\omega_i\rho\left(1+3\frac{c_i u}{c_s^2}+\frac{9}{2}\frac{\left(c_i u\right)^2}{c_s^4}-\frac{3}{2}\frac{\left(u\right)^2}{c_s^2}\right) \tag{19}$$

$$g_i^{eq}=\mathrm{T}\omega_i\left(1+3\frac{c_i u}{c_s^2}\right) \tag{20}$$

Where ω_i is the whiting factor, ρ is the lattice fluid density and u is the lattice fluid velocity

$$\omega_{i=0}=\frac{4}{9},\ \omega_{i=1-4}=\frac{1}{9},\ \omega_{i=5-8}=\frac{1}{36},\ c_\mathrm{s}=\frac{c_\mathrm{i}}{\sqrt{3}}$$

6.2. HYDRODYNAMIC BOUNDARY CONDITIONS

The unknown distribution functions at the inlet are calculated using the boundary condition proposed by Zou and He [46] as follows:

$$\rho_{in}=\frac{f_0+f_2+f_4+2\left(f_3+f_6+f_7\right)}{1-\mathrm{U_{in}}} \tag{21}$$

$$f_1=f_3+\frac{2}{3}\rho\mathrm{U_{in}} \tag{22}$$

$$f_5=f_7+\frac{1}{2}\left(f_4-f_2\right)+\frac{1}{6}\rho\mathrm{U_{in}} \tag{23}$$

$$f_8=f_6-\frac{1}{2}\left(f_4-f_2\right)+\frac{1}{6}\rho\mathrm{U_{in}} \tag{24}$$

At the outlet, a second order extrapolation scheme is used [47]:

$$f_3\left(x_{\mathrm{outlet}},j\right)=2\times f_3\left(x_{\mathrm{outlet}}-1,j\right)-f_3\left(x_{\mathrm{outlet}}-2,j\right) \tag{25}$$

$$f_6\left(x_{\text{outlet}}, j\right) = 2 \times f_6\left(x_{\text{outlet}} - 1, j\right) - f_6\left(x_{\text{outlet}} - 2, j\right) \tag{26}$$

$$f_7\left(x_{\text{outlet}}, j\right) = 2 \times f_7\left(x_{\text{outlet}} - 1, j\right) - f_7\left(x_{\text{outlet}} - 2, j\right) \tag{27}$$

The slip velocity condition is applied to the horizontal walls [48, 27]:
At the bottom wall:

$$\rho_{w-\text{bottom}} = f_0 + f_1 + f_3 + 2\left(f_4 + f_7 + f_8\right) \tag{28}$$

$$u_{x,y=0} = \lambda \frac{\left(4u_{x,y=1} - u_{x,y=2}\right)}{2 + 3\lambda} \tag{29}$$

$$f_2 = f_4 \tag{30}$$

$$f_5 = \frac{\rho_{\text{w-bottom}}\left(1 + u_{x,\text{y}=0}\right) - \left(f_0 + f_2 + f_4\right)}{2} - \left(f_1 + f_8\right) \tag{31}$$

$$f_6 = \frac{\rho_{\text{w-bottom}}\left(1 - u_{x,\text{y}=0}\right) - \left(f_0 + f_2 + f_4\right)}{2} - \left(f_3 + f_7\right) \tag{32}$$

At the top wall:

$$\rho_{w-\text{top}} = f_0 + f_1 + f_3 + 2\left(f_4 + f_7 + f_8\right) \tag{33}$$

$$\text{u}_{\text{x,y=H}} = \lambda \frac{\left(4u_{x,y=\text{H}-1} - u_{x,y=\text{H}-2}\right)}{2 + 3\lambda} \tag{34}$$

$$f_4 = f_2 \tag{35}$$

$$f_7 = \frac{\rho_{\text{w-top}}\left(1 - u_{x,\text{y}=\text{H}}\right) - \left(f_0 + f_2 + f_4\right)}{2} - \left(f_3 + f_6\right) \tag{36}$$

$$f_6 = \frac{\rho_{\text{w-top}}\left(1 + u_{x,\text{y}=\text{H}}\right) - \left(f_0 + f_2 + f_4\right)}{2} - \left(f_1 + f_5\right) \tag{37}$$

6.3. THERMAL BOUNDARY CONDITIONS

The temperature jump condition applied to the horizontal wall is obtained in a similar way to the slip velocity one [27, 48].
The temperature jump coefficient is defined as:

$$\text{C}_{\text{jump}} = \zeta \text{Kn}\left(\frac{2\gamma}{(\gamma + 1)Pr}\right)\lambda = \kappa\lambda \tag{38}$$

At the bottom wall

$$T_{x,y=0} = \frac{\mathrm{C}_{\mathrm{jump}}\left(4\mathrm{T}_{x,y=1} - \mathrm{T}_{x,y=2}\right) + 2T_{x,paroi}}{2 + 3C_{jump}} \tag{39}$$

$$g_2 = T_{x,y=0}\left(\omega(2) + \omega(4)\right) - g_4 \tag{40}$$

$$g_5 = T_{x,y=0}\left(\omega(5) + \omega(7)\right) - g_7 \tag{41}$$

$$g_6 = T_{x,y=0}\left(\omega(6) + \omega(8)\right) - g_8 \tag{42}$$

At the top wall

$$T_{x,y=\mathrm{H}} = \frac{\mathrm{C}_{\mathrm{jump}}\left(4\mathrm{T}_{x,y=\mathrm{H}-1} - \mathrm{T}_{x,y=\mathrm{H}-2}\right) + 2T_{x,paroi}}{2 + 3C_{jump}} \tag{43}$$

$$g_4 = T_{x,y=\mathrm{H}}\left(\omega(2) + \omega(4)\right) - g_2 \tag{44}$$

$$g_7 = T_{x,y=\mathrm{H}}\left(\omega(5) + \omega(7)\right) - g_5 \tag{45}$$

$$g_8 = T_{x,y=\mathrm{H}}\left(\omega(6) + \omega(8)\right) - g_6 \tag{46}$$

At the inlet, the flow is generated by a cold temperature given as follows:

$$g_1 = T_{inlet}\left(\omega(1) + \omega(3)\right) - g_3 \tag{47}$$

$$g_5 = T_{inlet}\left(\omega(5) + \omega(7)\right) - g_7 \tag{48}$$

$$g_8 = T_{inlet}\left(\omega(6) + \omega(8)\right) - g_6 \tag{49}$$

At the outlet, an extrapolation scheme is used [35]:

$$g_3\left(x_w, j\right) = 2 \times g_3\left(x_w - 1, j\right) - g_3\left(x_w - 2, j\right) \tag{50}$$

$$g_6\left(x_w, j\right) = 2 \times g_6\left(x_w - 1, j\right) - g_6\left(x_w - 2, j\right) \tag{51}$$

$$g_7\left(x_w, j\right) = 2 \times g_7\left(x_w - 1, j\right) - g_7\left(x_w - 2, j\right) \tag{52}$$

7. GRID INDEPENDENCY TEST AND CODE VALIDATION

In order to determinate the independent solution, different grids of 100 × 25, 200 × 50 and 400 × 100 for Re = 10, Kn = 0 and ϕ = 0% were explored. Results are

presented in Table 1, which shows the effect of mesh resolution on the $Nu_{average}$ of nanofluid through the two-dimensional microchannel. Based on the evolution of $Nu_{average}$ *versus* mesh resolution, the grid nodes 200 × 50 is selected for the next computations.

Table 1

Effect of the mesh resolution on the $Nu_{average}$ for Kn = 0, Re = 10 and ϕ = 0%

Mesh	100 × 25	**200 × 50**	200 × 50
$Nu_{average}$	9.85	**9.90**	9.94

The case of two-dimensional heated channel crossed with cold air (Pr = 0.71) was taken as a benchmark test in order to ensure that the obtained results are correct. The channel was heated from its top and bottom walls. In the first step, the velocity profile at different sections of the channel is compared with those obtained by Tang *et al.* [49] and Mohebbi *et al.* [50]. Based on the aforementioned comparisons, the present results show a good agreement. In addition, the fully-developed velocity is compared to the analytical solution ($U_{max} = U_{in} = 1.5$) (Fig. 2b).

The analytical solution for fully-developed flow between two parallel plates is defined as [51].

$$\frac{u}{u_{in}} = \frac{3}{2}\left(\frac{4y}{H} - \left(\frac{2y}{H}\right)^2\right) \tag{53}$$

Results agree with the analytical one. Besides, LBM findings are highly accurate.

8. RESULTS AND DISCUSSIONS

In the following sections, a numerical investigation has been carried out to appraise the effects of emerging parameters on the hydrodynamic and thermal characteristics and entropy generation inside a microchannel crossed by Cu-water nanofluid with a constant velocity and driven by a cold temperature at the inlet. The Patel model [52] for the nanofluid thermal conductivity and the Brinkman theoretical model for the dynamic viscosity [53] are adopted in the current study. Compared to both experimental and numerical findings, the Patel model has proven its consistency and quite good accuracy in numerous works [54, 55]. Calculations are performed using LBM in the slip flow regime. Particular efforts have been focused on the effects of the key parameters such as: Nanoparticles volume fraction (ϕ = 0%–4%), diameter size of Cu nanoparticles (d_p), Re number (Re = 5–100) and Kn number ($0–10^{-1}$).

8.1. EFFECT OF NANOPARTICLES VOLUME FRACTION AND DIAMETER SIZE

Figure 3 depicts the effects of the nanoparticles volume fraction (ϕ) on the $Nu_{average}$ (a) S_{gen} (b) and Be number (c) of the microchannel flow at different Re. At a given Re, it is found that the $Nu_{average}$ go up as ϕ develops.

The addition of nanoparticles to the pure fluid improves the thermal conductivity of the mixture inside the microchannel which improves the heat transfer rate. The $Nu_{average}$ enhances by 26.34 and 28.63% for Re = 5 and 100, respectively.

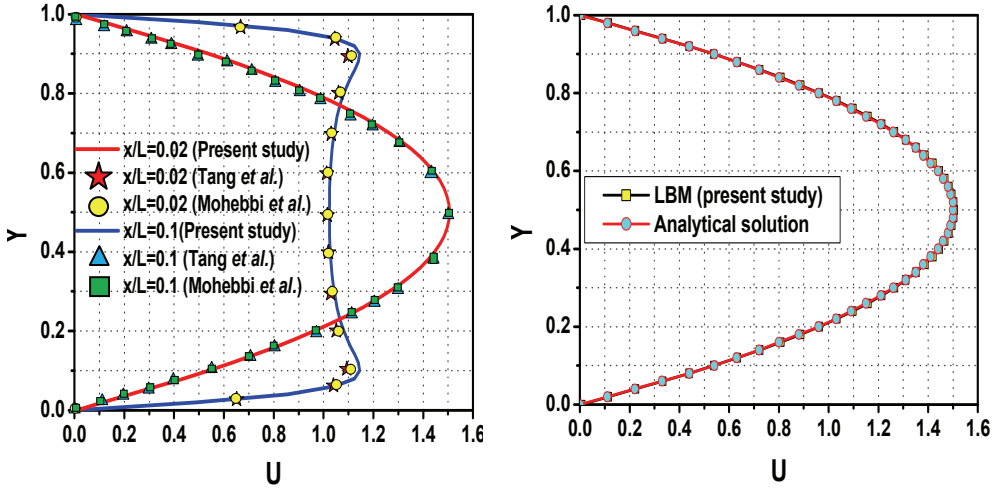

(a) (b)

Fig. 2 – A comparison between the velocity profile at different channel sections and those obtained by Tang *et al*. [49] and Mohebbi *et al.* [50] (a) and a comparison between a fully-developed velocity and the analytical exact solution (b).

The S_{gen} *versus* ϕ is illustrated in Fig. 3b. It is clear on the figure that the total entropy generation undergoes a slight reduction as ϕ grows. Besides, the ϕ augmentation affects the thermo-physical proprieties of the nanoliquid. The dynamic viscosity expands which favors the augmentation of the fluid friction irreversibility. The influence of ϕ on Be number, presented in Fig. 3c, is used to identify the heat transfer mode. For all values of Re, the Be number indicates that the conduction mode is the dominant one. At low Re, the Be number remains unchanged with respect to ϕ. While as Re raises, the Be number grows slightly with respect to ϕ. The improvement is 1.97% and 4.3% for Re=50 and 100, respectively.

Figure 4 illustrates the variation of $Nu_{average}$ *versus* the diameter size of Cu nanoparticles for various values of Kn and Re. It is noted that the maximum heat transfer occurs at low values of d_p and great values of Kn for all the value of Re. The use of microchannel in a variety of emerging application such us cooling electronics device is recommended with lower values of d_p and high values of Kn.

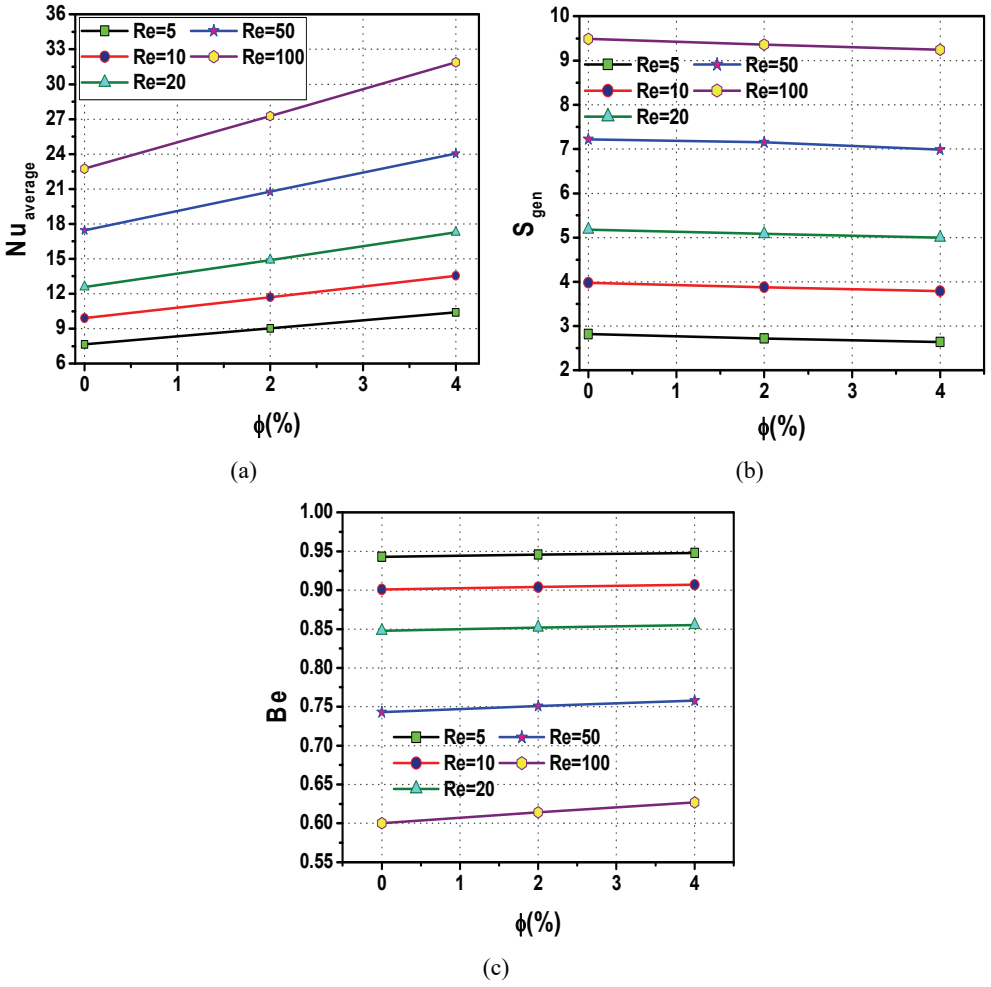

Fig. 3 – Variation of $Nu_{average}$ (a), S_{gen} (b) and Be (c) as a function of nanoparticles volume fraction (ϕ) for different Re number for d_p = 25 nm and Kn = 0.

8.2. EFFECT OF VISCOUS FORCES

The profile of the dimensionless horizontal velocity for nanofluid along the microchannel centerline is depicted in Fig. 5 (left) confirms that a fully-developed

flow is reached more rapidly at lower values of Re ($U_{max} = U_{in} = 1.5$). It is also observed that by increasing Reynolds number, the velocity field is developed later.

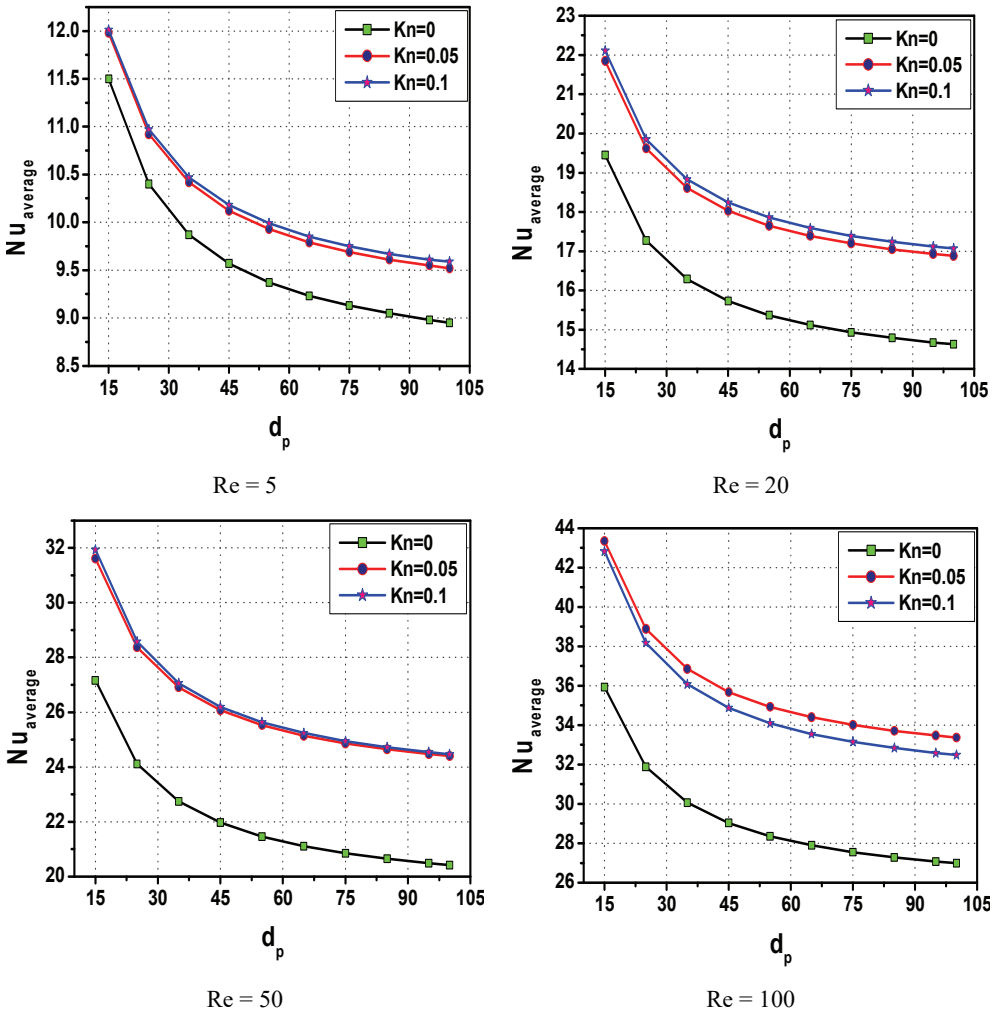

Fig. 4 – Variation of the $Nu_{average}$ as a function of the diameter size of Cu nanoparticles for different Re and Kn for $\phi = 4\%$.

Figure 5 (right) shows that the mixture temperature in the middle section of the microchannel develops at low Re. As Re growth, the temperature decrease until reaches zero for Re = 50 and 100. Moreover, at low Re, the flow velocities is very low. Consequently, the heat exchange between the partially heated microchannel walls and the nanoliquid takes enough time. Increasing Re, the nanofluid motion

inside the microstructure becomes very rapidly due to the augmentation of flow velocity. This reason noticeably affects the thermal behavior of the nanofluid.

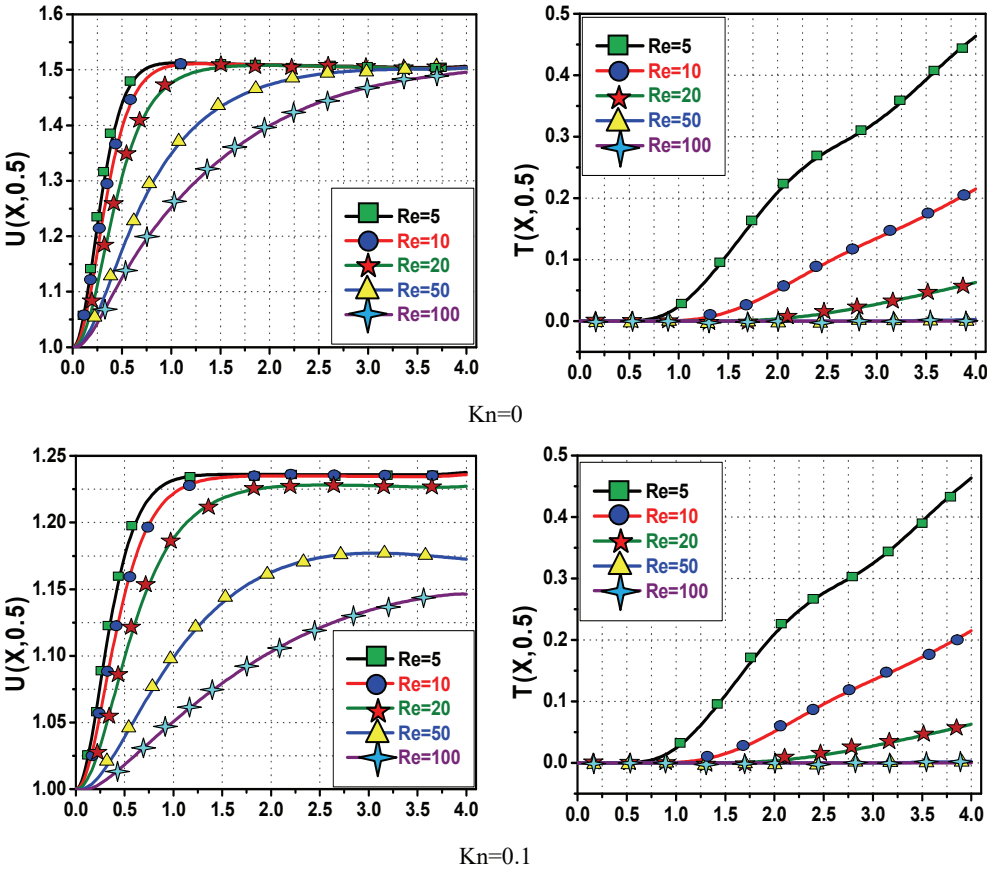

Fig. 5 – Velocity (left) and Temperature (right) profiles along the horizontal axis for the different Re and Kn.

Figure 6 illustrates the effect of Re on the $Nu_{average}$ (a), S_{gen} (b) and Be number (c) on the slip flow regime ($0 < Kn < 0.1$). It is clear that the increase of Re enhances the heat transfer by 67.4% and 71.26% for $Kn = 0$ and 0.1, respectively (Fig. 6a). The raise of Re is accompanied by an augmentation in velocity of the microflow which improves the heat exchange between the walls and the nanofluid. Consequently, the heat transfer rate enhances. The variation of S_{gen} *versus* Re is depicted in Fig. 6b. The figure demonstrates that the growth of Re causes the augmentation of the total entropy generation inside the microchannel. Besides, as Re increase the motion of the nanoliquid expands due to the development of the velocity strength which improves of the nanofluid thermal conductivity near the

partially microchannel walls. Consequently, the entropy due to heat transfer enhances. Figure 6c reveals to the evolution of Be number *vs* Re. The development of the total entropy generation reduces the Be number inside the mico-medium.

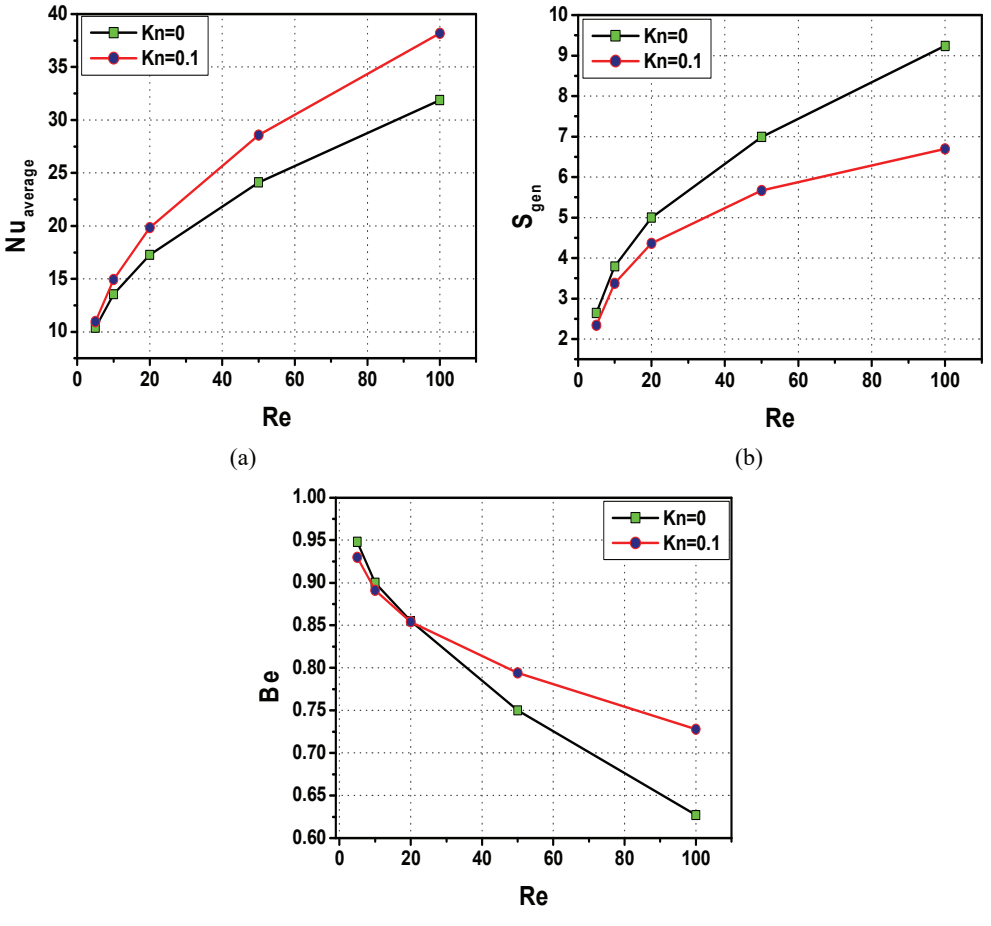

Fig. 6 – Variation of $Nu_{average}$ (a), S_{gen} (b) and Be (c) as a function of Re for different Kn and d_p=25 nm.

8.3. EFFECT OF KNUDSEN NUMBER

Figure 7 describes the evolution of the developed velocity profile along the vertical centerline according to Kn for different Re. The figure reveals the rise of Kn reduces the velocity in the core region of the microchannel and improves this one near the bottom and top walls. This is due to the slip condition applied to the microchannel walls. The rise of Re does not affect the developed velocity profile.

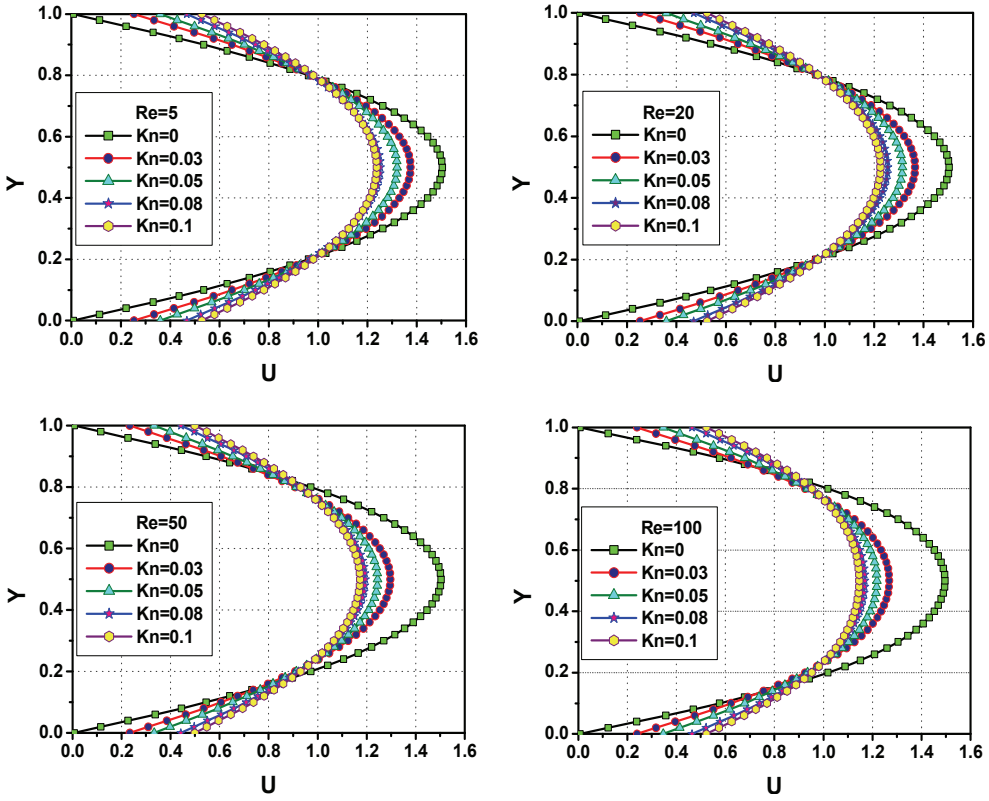

Fig.7 – Developed velocity profile of nanoliquid at the vertical centerline of the microchannel for different Kn and Re.

To better understand the temperature jump boundary conditions, Fig. 8 illustrates the temperature profiles of the nanofluid at $X = L/4$ (left) and $X = 3 \times L/4$ (right) along the vertical axis of the microchannel for different Kn and Re. It is seen on this figure that the increase of Kn leads to a higher temperature jump near the partially heated walls which results in a decrease of the temperature gradient. As Re raises the temperature goes down in the core region of the microchannel. Besides, at high Re, the velocity of nanofluid multiplies and the flow develops rapidly. Consequently, the mixture inside the microchannel does not have enough time to contact with the partially heated walls, which causes the reduction of nanofluid temperature.

Figure 9 presents the variation of the velocity of the Cu-water nanofluid along the horizontal axis of the microchannel for different Kn and Re. We can deduct from the figure that the axial velocity is considerably affected by the increase in Kn for all Re numbers. For each Re, the mid-height velocity reaches more

rapidly its maximum (U_{max}=1.5) at lower values of Re and Kn = 0. A considerable decrease of the mid-height velocity is observed when Kn rises.

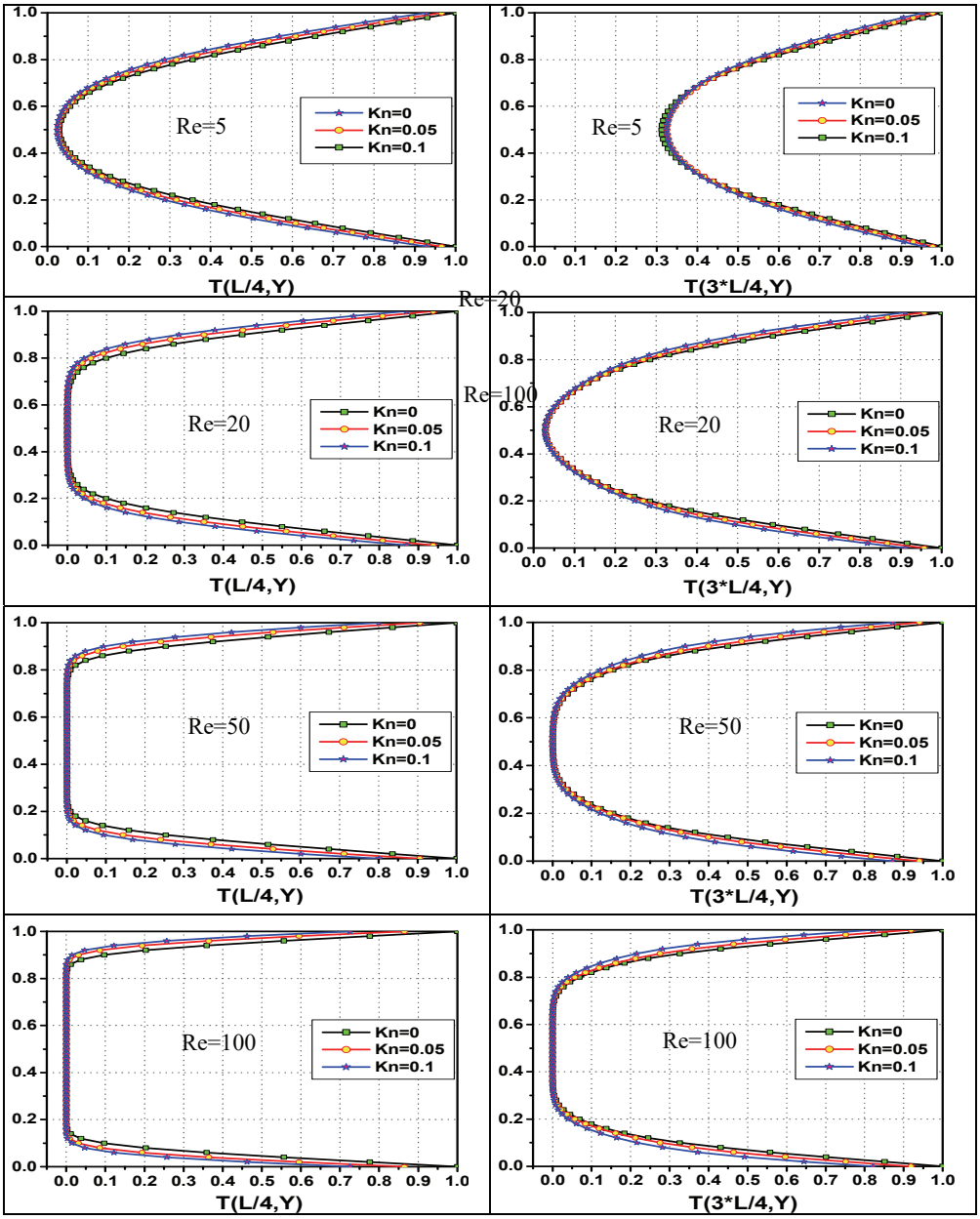

Fig. 8 – Temperature profiles of nanoliquid at $X = L/4$ (left) and $X = 3 \times L/4$ (right) of the microchannel for different Kn and Re.

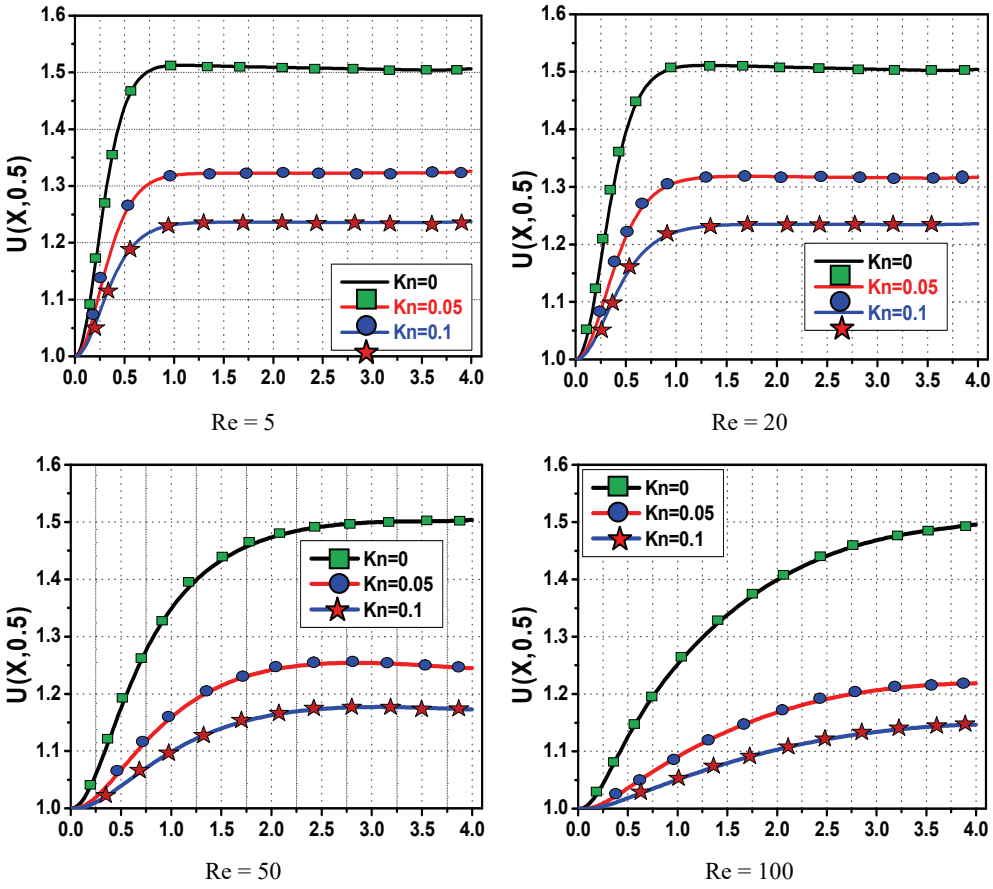

Fig. 9 – Velocity profiles along the horizontal axis for different Re and Kn.

Figures 10 and 11 delineate the results for slip velocity (U_s) and temperature jump (T_{jump}) variations for different Kn and Re numbers. As can be seen from this figure, increasing Kn number leads to improve in slip velocities and temperature jump in the developing region. It can be observed also that the slip velocity is at its maximum near the wall at microchannel inlet and then it is reduced very slightly along the microchannel walls until reaching a fixed value. As for the temperature jump, the increase is remarkable at the heated zone of the walls. This is due to the temperature jump condition applied to the partially heated microchannel walls.

Figure 12 depicts the impact of Kn number on the $Nu_{average}$ (a), S_{gen} (b) and Be number (c) for different Re numbers. The variation of $Nu_{average}$ *versus* Kn for Cu-water nanofluid delineated in Fig. 12a shows that the heat transfer is enhanced with the increase in Kn for Re < 50 owing to the development of the slip velocity and temperature jump near the walls. For Re = 100, it is seen that the $Nu_{average}$

enhances for Kn < 0.05, then its remains unchanged for 0.05 < Kn < 0.08, after this value the heat transfer undergoes a slight decrease.

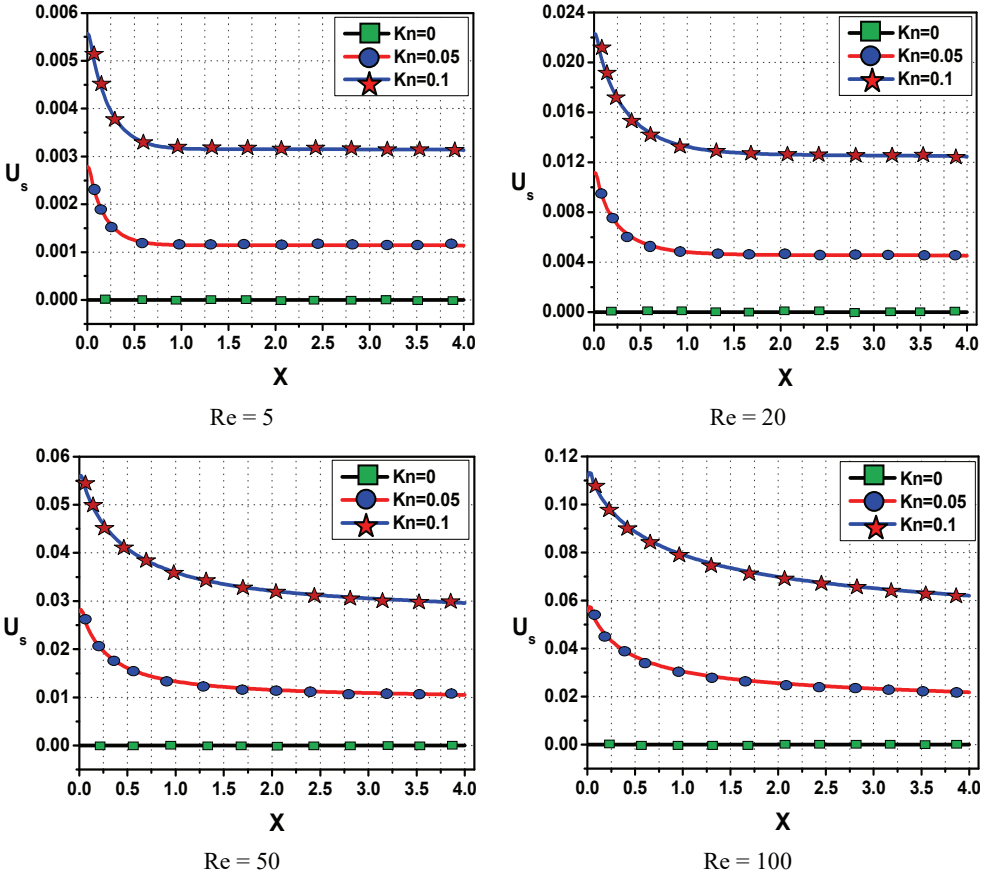

Fig. 10 – Slip velocity along the microchannel wall for different Re and Kn.

The total entropy generation under the effect of Kn is presented in Fig. 12b. The augmentation of Kn noticeably reduces the irreversibility factor inside the micro medium. This reduction is more pronounced for high values of Re. The increase of Kn increase the slip velocity and the temperature jump near the partially heated microchannel wall which go up the motion of the mixture inside the confined medium. That is why, the entropy declines, also due to the fluid friction, which affects the total value of S_{gen}. Figure 12c reveals the variation of Be number under the effect of Kn. It is noted from the figure that the conduction mode is the dominant one. At low Re, the Be number remains constant as Kn growth (Re<20). For Re>50, the Be number enhance when Kn expands.

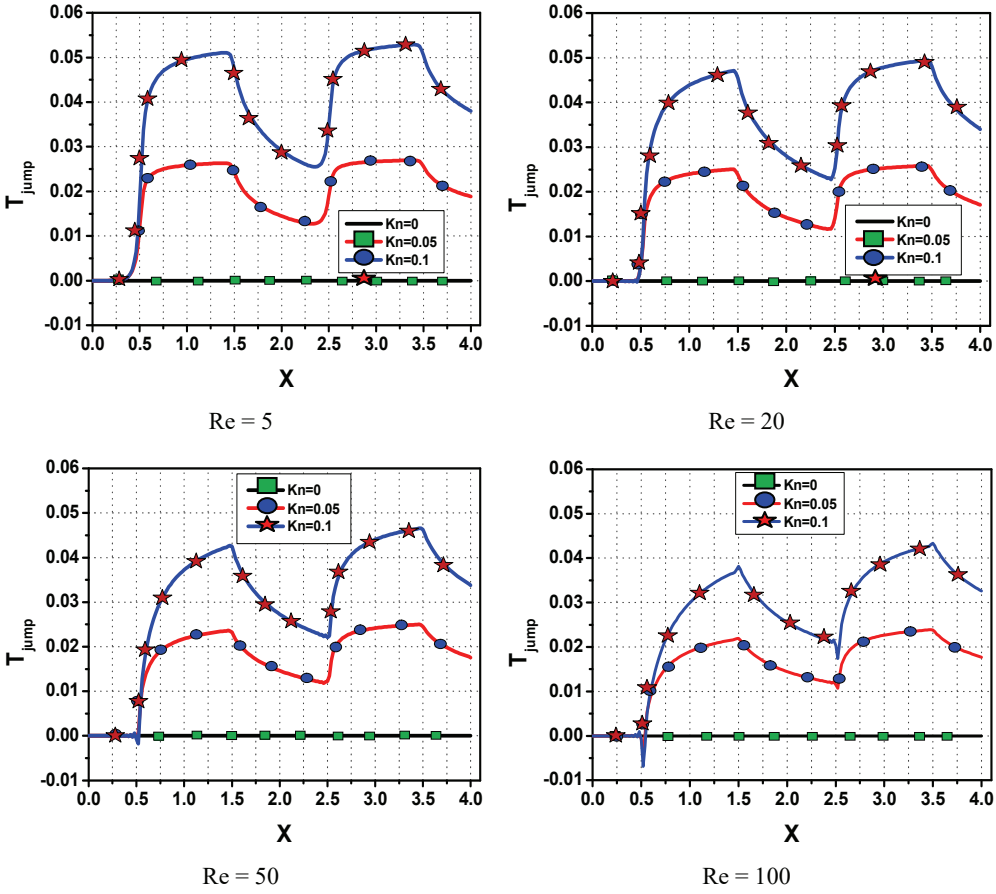

Fig. 11 – Temperature jump along the microchannel wall for different Re and Kn.

9. CONCLUSION

A numerical investigation has been performed in a microchannel partially heated from the horizontal walls, flowed with a cold nanoliquid at the inlet and crossed with Cu-water nanofluid. LBM is used for resolving the Navier-Stokes equations. Slip velocity and temperature jump conditions are applied to the lower and upper microchannel walls in the slip flow regime. The controls of the microflow characteristics are studied under the effect of several parameters. The most important findings are concluded as follow:

– As ϕ growth, the $Nu_{average}$, and S_{gen} increases and decreases respectively. Be > 0.5 for all value of Re with respect to ϕ. Consequently, the conduction mode is the dominant one.

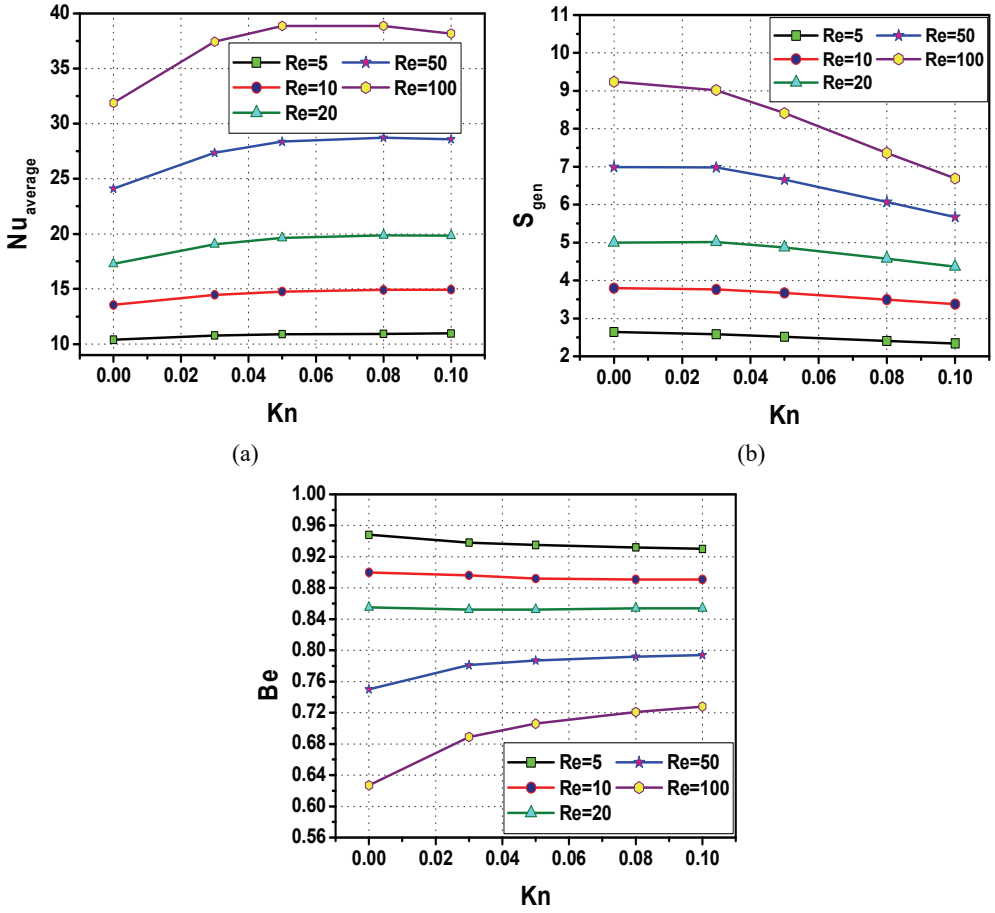

Fig. 12 – Variation of $Nu_{average}$ (a), S_{gen} (b) and Be (c) *versus* Kn for different Re, d_p = 25 nm and ϕ = 4%.

- The increase of Cu nanoparticles diameter size reduces the heat transfer rate.
- The augmentation of viscous force affects the hydrodynamic and thermal behavior of the flow. It also found that this factor improves the heat transfer and entropy generation and decreases the Be number.
- The rise in Kn leads to decline of the velocity in the core region and it expansion near the microchannel walls.
- The horizontal velocity drops by increasing Kn for all value of Re.
- The slip velocity takes a maximum value in the walls part near the inlet and then declines along the microchannel axis for Kn > 0. The temperature jump is at its maximum near the heated zone.
- The augmentation of Kn develops the slip velocity and temperature jump.

– $Nu_{average}$ enhances with Kn for lower value of Re while for great value of Re the $Nu_{average}$ increases for $Kn \leq 0.05$, while for $0.05 \leq Kn \leq 0.08$ the heat transfer remains constant, then it drops to $Kn \geq 0.08$. The total entropy generation expands with Kn, this behavior is more pronounced for higher value of Re. The Be number is unchanged for low value of Re with respect to Kn, but at higher value of Re the Be improves with Kn.

Disclosure statement: The authors declare that there is no conflict of interest regarding the publication of this article and there were no external funding sources for this study.

REFERENCES

1. X. Nie, G. D. Doolen, and S. Chen, J. stat. phy. **107**, 279–289 (2002).
2. C. M. Ho, Annu. Rev. Fluid Mech. **30**, 579–612 (1998).
3. Y. Xuan, Q. Li, and M. Ye, Int. J. Therm. Sci. **46**, 105–111 (2007).
4. T. Adams, S. Abdel-Khalik, S. Jeter, and Z. Qureshi, Int. J. Heat and Mass Transfer. **41**, 851–857 (1998).
5. Y. Elguennouni, M. Hssikou, J. Baliti, and M. Alaoui, Math. Probl. Eng. **2020**, 1–13 (2020).
6. H. H. Afrouzi, M. Hosseini, D. Toghraie, E. Mehryaar, and M. Afrand, Physica A: Stat. Mech. App. **553**, 124–669 (2020).
7. M. Kalteh and S. S. Abedinzadeh, Iranian J. of Sci. and Technol., Trans. Mech. Eng. **42**, 23–34 (2018).
8. M. Afrand, A. Karimipour, A. A. Nadooshan, and M. Akbari, Physica E: Low-Dimens. Syst. and Nanostructures. **84**, 474–481 (2018).
9. A. Karimipour, A. Taghipour, and A. Malvandi, J. Magn. Magn. Mater. **419**, 420–428 (2016).
10. A. Karimipour and M. Afrand, Proceedings of the Institution of Mechanical Engineers, Part C: J. Mecha. Eng. Sci. **230**, 1921–1936 (2016).
11. A. Karimipour, A. D'Orazio, and M. S. Shadloo, Physica E: Low-Dimens. Syst. Nanostructures. **86**, 146–153 (2017).
12. A. Karimipour, Int. J. Therm. Sci. **91**, 146–156 (2015).
13. F. Verhaeghe, L. S. Luo, and B. Blanpain, J. Comput. Phy. **228**, 147–157 (2009).
14. X. Niu, C. Shu, Y. Chew, Comput. Fluids. **36**, 273–281 (2007).
15. Y. Zhang, G. Xie, A. Karimipour, and B. Sundén, Numer. Heat Transfer, Part A: Applications. **78**, 159–179 (2020).
16. A. D'Orazio, M. Corcione, and G. P. Celata, Int. J. Therm. Sci. **43**, 575–586 (2004).
17. M. Mozaffari, A. Karimipour, and A. D'Orazio, J. Therm. Anal. Calorim. **137**, 229–243 (2019).
18. M. Mozaffari, A. D'Orazio, A. Karimipour, A. Abdollahi, and M. R. Safaei. Int. J. Numer. Methods Heat Fluid Flow. **30**, 3371–3398 (2019).
19. R. Zarita and M. Hachemi, Front. Heat Mass Trans. (FHMT). **12 (**2018).
20. A. Raisi, B. Ghasemi, and S. M. Aminossadati. Num. Heat Transfer, Part A: Applications. **59**, 114–129 (2011).
21. A. Arabpour, A. Karimipour, D. Toghraie, and O. A. Akbari, J. Therm. Anal. Calorim. **131**, 2975–2991 (2018).
22. R. L. Monaledi and O. D. Makinde, J. Therm. Anal. Calorim. 2020:1–11.
23. S. Sindhu, B. Gireesha, and G. Sowmya, Int. J. Numer. Methods Heat Fluid Flow. **30**, 5063–5085 (2020).
24. A.A.A.A. Al-Rashed, A. Shahsavar, S. Entezari, M. A. Moghimi, S. A. Adio, and T. K. Nguyen, App. Therm. Eng. **155**, 247–258 (2019).
25. G. Huminic and A. Huminic, J. Mol. Liq. **302**, 112–533 (2020).

26. M. M. Awad, Adv. Mech. Eng. **7**, 1687814015590297 (2015).
27. Z. W. Tian, C. Zou, Z. H. Liu, Z. L. Guo, H. J. Liu, and C. G. Zheng, Int. J. Mod. Phy. C. **17**, 603–614 (2006).
28. R. Djebali, A. Jaouabi, T. Naffouti, and S. Abboudi, Int. J. Numer. Methods Heat Fluid Flow. **30**, 742–768 (2020).
29. S. N. Shashikumar, B. J. Gireesha, B. Mahanthesh, B. C. Prasannakumara, and A. J. Chamkha, Int. J. Numer. Methods Heat Fluid Flow. **29**, 3638–3658 (2019).
30. S. Marzougui, F. Mebarek-Oudina, A. Assia, M. Magherbi, Z. Shah, and K. Ramesh, J. Therm. Anal. Calorim. **143**, 2203–2214 (2021).
31. M. A. Abbassi and J. Orfi, J. Thermophys. Heat Transfer. **32**, 1059–1071 (2018).
32. W. Al-Kouz, A. Al-Muhtady, W. Owhaib, S. Al-Dahidi, M. Hader, and R. Abu-Alghanam, Entropy. **21**, 103 (2019).
33. R. Djebali and M. El Ganaoui, Comp. Modeling. Eng. Sci. **71**, 179 (2011).
34. R. Djebali and H. Sammouda, and M. El Ganaoui, Adv. Appl. Math. Mech. **2**, 587–608 (2010).
35. T. Naffouti and R. Djebali, Comp. Modeling Eng. Sci. (CMES). **88**, 211–227 (2012).
36. M. A. Abbassi, R. Djebali, K. Guedri, J. Therm. Eng. **4**, 2018–2036 (2018).
37. M. Ferhi, R. Djebali, W. Al-Kouz, S. Abboudi and A. J. Chamkha, Heat Transfer. **50**, 126–144 (2021).
38. M. Ferhi and R. Djebali, Int. J. Numer. Methods Heat Fluid Flow. **30**, 4529–4562 (2020).
39. M. Ferhi, R. Djebali, S. Abboudi, and H. Karroubi, J. Therm. Anal. Calorim. **138**, 3065–8308 (2019).
40. M. Ferhi, R. Djebali, S. Abboudi, CFD Lett. **11**, 1–27 (2019).
41. R. Djebali, B. Pateyron, M. El Ganaoui, Surf. Coatings Techn. **220**, 157–163 (2013).
42. R. Djebali, M. ElGanaoui, T. Naffouti, Comp. Model. Eng. Sci. **84**, 499–527 (2012).
43. R. Djebali, M. El Ganaoui, B. Pateyron, Prog. Computa. Fluid Dynamics, an Int. J. **12**, 270–278 (2012).
44. R. Djebali, M. El Ganaoui, B. Pateyron, H. Sammouda, Defect and Diffusion Forum. **312–315**, 1167–1171 (2011).
45. R. Djebali, M. ElGanaoui, A. Jaouabi, B. Pateyron, Int. J. Therm. Sci. **100**, 229–239 (2016).
46. Q. Zou and X. He, Phy. Fluids. **9**, 1591–1598 (1997).
47. A. Mohamad, Dept. of mechanical and manufacturing engineering, Schulich School of Engineering, the University of Calgary, Alberta, Canada (2011).
48. S. B. Çelik, Graduate School of Natural and Applied Science, Thesis (2012).
49. G. Tang, W. Tao, and Y. He, Int. J. Mod. Phy. B **17**, 183–187 (2003).
50. R. Mohebbi, M. Rashidi, M. Izadi, N. A. C. Sidik, and H. W. Xian, Int. J. Heat and Mass Transfer. **117**, 1291–1303 (2018).
51. F. Durst, Springer Science & Business Media (2008).
52. H. E. Patel, T. Sundararajan, T. Pradeep, A. Dasgupta, N. Dasgupta, and S. K. Das, Pramana. **65**, 863–869 (2005).
53. H. Brinkman, The J. Chemi. Phy. **20**, 571–571 (1952).
54. R. Djebali, Rom. J. Phys. **65**, 122 (2020).
55. R. Djebali, Rom. Rep. Phys. **73**, 106 (2021).